Published in final edited form as:
Chem Biol. 2013 August 22; 20(8): 973–982. doi:10.1016/j.chembiol.2013.06.008.

Structure Based Design of Covalent Siah Inhibitors

John L. Stebbins[1,2], **Eugenio Santelli**[1,2], **Yongmei Feng**[1], **Surya K. De**[1,2], **Angela Purves**[1,2], **Khatereh Motamedchaboki**[3], **Bainan Wu**[1,2], **Ze'ev A. Ronai**[1], **Robert C. Liddington**[1,2], and **Maurizio Pellecchia**[1,2,*]

[1]Signal Transduction Program and Cell Death Program, Cancer Center, Sanford-Burnham Medical Research Institute, 10901 North Torrey Pines Road, La Jolla, CA 92037, USA

[2]Infectious and Inflammatory Disease Center, Sanford-Burnham Medical Research Institute, 10901 North Torrey Pines Road, La Jolla, CA 92037, USA

[3]Proteomics Facility, Sanford-Burnham Medical Research Institute, 10901 North Torrey Pines Road, La Jolla, CA 92037, USA

Abstract

The E3 ubiquitin ligase Siah regulates key cellular events that are central to cancer development and progression. A promising route to Siah inhibition is disrupting its interactions with adaptor proteins. However, typical of protein-protein interactions, traditional unbiased approaches to ligand discovery did not produce viable hits against this target, despite considerable effort and a multitude of approaches. Ultimately, a rational structure-based design strategy was successful for the identification of novel Siah inhibitors in which peptide binding drives specific covalent bond formation with the target. X-ray crystallography, mass spectrometry and functional data demonstrate that these peptide-mimetics are efficient covalent inhibitors of Siah and antagonize Siah-dependent regulation of Erk and Hif signaling in cell. The strategy proposed may result useful as a general approach to the design of peptide-based inhibitors of other protein-protein interactions.

INTRODUCTION

Seven in Absentia (Sina) is a *Drosophila* protein that targets Tramtrack, a transcription factor involved in fly eye development, for degradation (Tang et al., 1997). Siah1 and 2 are the mammalian orthologues of Sina, which are highly conserved across species (Della et al., 1993). Siah1 and Siah2 are the products of separate genes, which are activated by distinct mechanisms, yet are highly homologous (85% identity) and target common substrates (House et al., 2009). Siah is a RING finger E3 ubiquitin ligase implicated in diverse biological processes, such as p38/JNK/NF-kB signaling pathways (Habelhah et al., 2002; Habelhah et al., 2004; Nadeau et al., 2007; Nakayama et al., 2004; Zhang et al., 1998), DNA damage (Winter et al., 2008), estrogen signaling (Frasor et al., 2005), programmed cell death (Roperch et al., 1999; Xu et al., 2006), Ras/Raf pathway (Nadeau et al., 2007; Schmidt et al., 2007), mitosis (Bruzzoni-Giovanelli et al., 1999), and hypoxia (Nakayama et al., 2004; Nakayama et al., 2009).

*To whom correspondence should be addressed: mpellecchia@sanfordburnham.org.

The crystal structure of Siah1 lacking the RING domain (Siah1-ΔRING) revealed a dimeric organization (Figure 1a) which has been linked with Siah activity (Santelli et al., 2005), including self and targeted ubiquitination and degradation (Ahmed et al., 2008; Moller et al., 2009). Siah binds some of its substrates directly, whereas others require adaptor proteins such as Siah-interacting protein (SIP) (Matsuzawa and Reed, 2001) and phyllopod (Boulton et al., 2000; Dong et al., 1999; Li et al., 1997; Tang et al., 1997).

A number of Siah2 substrates, and the signaling pathways regulated by them, including TRAF2 (JNK/p38/NF-κB) (Habelhah et al., 2002), Sprouty2 (Raf/Ras signaling) (Nadeau et al., 2007), and PHD1/3 (hypoxia) (Nakayama et al., 2004), have been implicated in cancer development and progression (Fernandez-Medarde and Santos, 2011; Semenza, 2010). Genetic inhibition of Siah1/2 using RNA interference in tumor cell lines resulted in suppression of the development of melanoma, prostate, pancreatic, mammary, and lung tumors (Ahmed et al., 2008; Bedogni and Powell, 2009; Davies et al., 2002; Moller et al., 2009; Nakayama et al., 2009; Qi et al., 2010a; Qi et al., 2008; Schmidt et al., 2007; Shah et al., 2009). Accordingly, Siah2 expression and activity is upregulated in these tumors, in both xenografts and genetic mouse models (Ahmed et al., 2008; Confalonieri et al., 2009; Scortegagna et al., 2011). In addition, it has been reported that Siah directly interacts and ubiquitylates synphilin-1 and that Siah is present in Lewy bodies, presumably providing a link to its possible role in Parkinson's disease (Avraham et al., 2005; Liani et al., 2004; Nagano et al., 2003; Szargel et al., 2009). Collectively, these observationssuggest that Siah inhibitors could have significant therapeutic value.

In recent years, the search for an inhibitor of Siah has focused on the adaptor *Drosophila* protein phyllopod. Moller and colleagues discovered that Siah inhibitory properties resided in the first 130 amino acids of *Drosophila* phyllopod (PHYL 1-130). Overexpression of PHYL 1-130 inhibits Siah-induced substrate degradation (Moller et al., 2009), breast cancer progression (Moller et al., 2009), reduced melanoma metastasis (Qi et al., 2008) and prostate tumor development and metastasis (Qi et al., 2010a). Subsequently, House and colleagues identified a 23-residue peptide derived from the *Drosophila* phyllopod protein (Table 1) that binds with low micromolar affinity to the substrate-binding domain of Siah (House et al., 2003; House et al., 2006). A cell penetrating version of PHYL 108-130 inhibits Siah ubiquitin ligase activity in cell culture (Moller et al., 2009). Therefore, independent lines of evidence suggest that PHYL-related sequences could provide the basis for development of therapeutics targeting Siah (House et al., 2003; House et al., 2006; Moller et al., 2009; Qi et al., 2010b).

In principle this peptide provides an excellent tool for the development of a High Throughput Screening (HTS) campaign aimed at the identification of small molecule Siah inhibitors. However, typical of drug discovery campaigns that target protein-protein interactions, these efforts did not result in any viable hits.

We previously reported the high-resolution (2.2 Å) crystal structure of Siah1 in complex with a peptide from Siah-interacting protein (SIP), which contains the PXAXVXP consensus binding sequence also present in PHYL 108-130 (Santelli et al., 2005). A low-resolution (3 Å) structure of Siah1 in complex with PHYL 108-130 was also reported (House et al., 2006), while we report here the structure of Siah1 in complex with a smaller PHYL-derived peptide (Figure 1a). As PHYL 108-130 binds in an identical mode as SIP, we used its sequence as the starting point for developing high-affinity peptide-based inhibitors.

As a result of several successful cases of effective therapeutics, drugs that bind their target by means of covalent attachment have recently come back into favor following initial fears by the pharmaceutical industry about possible off-target effects (Singh et al., 2011). In

recent years more emphasis has been placed on combining the distinct strengths of covalent and non-covalent modes of drug action with the design of compounds that carefully balance reactivity with specific target complementarities. With the notable exception of suicide protease inhibitors, peptides have been largely underexplored in this regard; yet make an excellent platform for the development of this class of therapeutics. We report here on the rational development of potent, selective, and irreversible peptide-based inhibitors against Siah. We also show X-ray, mass spectroscopy and functional data for this novel class of molecules targeting Siah.

RESULTS AND DISCUSSION

Because the residues in Siah1 and Siah2 involved in phyllopod binding are conserved, we used constructs of either isoform interchangeably in the various binding and cellular assays. First, we exploited the PHYL 108-130/Siah interaction for the development of a robust and reproducible lanthanide-based heterogeneous displacement assay (DELFIA) platform that could be used in HTS campaigns aimed at identification of Siah inhibitors. Initially we screened 16,009 compounds from an in house compound collection using the DELFIA assay. However, this screen revealed no viable hits when tested at 50 μM. In addition, we tested two large combinatorial libraries of peptides from the Torrey Pines Institute for Molecular Studies (two positional scanning libraries of hexa-peptides and deca-peptides). However, after deconvolution of the mixtures, re-synthesis, and assessing dose-response relationship, no viable hits were identified. We concluded that the rather large and shallow PHYL binding surface of Siah1 is an unlikely fit for “drug-like” small molecule inhibitors. The non-drugabbility of the PHYL-binding pocket is further demonstrated by a subsequent NMR-based fragment screen of a library of approximately 500 scaffolds. For this task, we obtained ^{13}C-Methionine-labeled-Siah2 and used chemical shift changes in ^{13}C and/or ^{1}H using either 2D [^{13}C, ^{1}H] HSQC spectra or 1D ^{13}C-filtered ^{1}H NMR spectra in absence or presence of test ligands. These spectra are sensitive to binding because of the presence of residue Met 180 in the PHYL binding pocket. Again, no viable fragment hits were found. Similarly, in a parallel effort employing the phyllopod homolog plectin, a screen from the SBMRI MLPCN center of the NIH compound library of approximately 300,000 compounds using a rhodamine-plectin based fluorescence polarization displacement assay (FPA) and secondary time-resolved fluorescence resonance energy transfer displacement assay (TR-FRET) assays also revealed no viable hits (see http://pubchem.ncbi.nlm.nih.gov bioassays AIDs 1817see http://pubchem.ncbi.nlm.nih.gov bioassays AIDs 1826, 2127 and 2141 for details).

Hence, we redirected our efforts into more rational design of PHYL mimetics. We first sought to define the region of the 23-mer PHYL 108-130 peptide that was necessary and sufficient for binding to Siah1. Using the DELFIA assay we identified the 13-mer, KLRPVAMVRPTVR (BI-107D1; Table 1) as a suitable starting point for optimization, given that it retained similar displacement activity of the longer peptide. The BI-107D1 sequence comprises the residues that form close contacts with Siah in the crystal structures of Siah-peptide complexes (House et al., 2006; Santelli et al., 2005). However, initial attempts to derive mimetics of BI-107D1 with improved affinity for Siah were unsuccessful (Table S1).

Noticeable in the Siah1 crystal structures (House et al., 2006; Santelli et al., 2005) is the existence of two small hydrophobic pockets, one adjacent to the site of binding of the methyl side chain of PHYL residue Ala118 (P1 in Figure 1b) and the other corresponding to the binding site adjacent to PHYL residue Thr123 (P2 in Figure 1b). In an attempt to exploit these sub-pockets and to improve potency of the peptide, we introduced different amino acids at these positions with a variety of side chain lengths and geometry (Table 1 and

supplementary Table S1). Of the peptides produced in our initial studies only BI-107E1 (IC_{50} = 2 μM; Table 1), an ethyl-glycine substitution at position 118, efficiently competed for binding with the reference PHYL peptide. To better understand the binding mode of this peptide we determined the crystal structure of BI-107E1 bound to Siah1 at 3 Å resolution. The structure demonstrated that the extra methyl group was accommodated without significant changes in the peptide binding mode or distortions in the protein (Figures 1b and 1c).

Similarly, substitution of Thr123 with more hydrophobic residues that reached farther into the P2 pocket resulted in peptides with modestly increased affinities (BI-107E12 and BI-107F1, Table 1). Despite this limited success, further simple amino acid replacements resulted in peptide-mimetics with dramatically reduced binding affinities for Siah (Table S1) and thus making this simple route not a viable strategy for improvement; this result is not entirely surprising given the already optimal fit between the PHYL peptide and the shallow binding pocket on Siah.

Recent efforts aimed at improving the binding affinity of small molecule drugs for their receptor involve the introduction of a mildly reactive group (usually a Michael acceptor such as an acrylamide) designed to react selectively with a cysteine thiol group present in the target binding site. This approach, originally proposed by Shokat & coworkers to obtain selective inhibitors of kinases (Maly et al., 2004), is currently exploited in several inhibitor optimization efforts when a cysteine residue is proximal to the binding site and has led to advanced and orally active clinical candidates (Singh et al., 2011). In an attempt to derive more potent and selective Siah inhibitors we applied this approach to BI-107F1. An initial proof-of-concept approach consisted in replacing the side chain of BI-107F1 Ala118 with a suitably reactive “warhead” that could form a covalent bond with a cysteine residue present in the P1 pocket of Siah (Figure 2a). Although wild-type Siah contains no such cysteine at this position, simple modeling suggested that by mutating Siah Thr156 to cysteine and adding the warhead, Dap-acrylamide (Dap-acm), in lieu of Ala118, binding of the resulting BI-117C3 (Table 1, Figure 2a) compound in its standard configuration would bring the acrylamide into close apposition with the cysteine sulfhydryl group. Nucleophilic attack by the cysteine sulfur on the acrylamide alkene bond (Michael addition) could then ensue and result in the formation of a covalent thioether bond between Siah and the peptide. Indeed, we found that BI-117C3 efficiently displaced PHYL 108-130 from the T156C Siah1 mutant, but not from wild-type Siah1, with an IC_{50} value of 0.006 μM (Table 1). Of note is that IC_{50} values of covalent inhibitors are obviously relative to the assay conditions and incubation times. Hence, the reported IC_{50} values for these covalent compounds refer to our standard DELFIA protocol (see methods) and therefore serve only as way of rank ordering the relative potency of the compounds.

We next solved the crystal structure of BI-117C3/T156C Siah1 complex at 2.8 Å resolution. The map reveals continuous electron density that is fully consistent with a covalent thioether bond linking the modified peptide to Cys156 (Figures 2b and c). The bond is formed with ~100% efficiency, as judged by refined atomic B-factors. Moreover, the core PV(Dap-acm)MVRP motif is bound to Siah in its standard orientation without significant distortion of the substrate-binding domain or the disposition of the second zinc finger domain while the newly introduced tryptophan occupies the P2 pocket (Figures 2b and c). To confirm the covalent modification of Siah1 we used MALDI-TOF mass spectrometry, which demonstrated the expected mass increase when BI-117C3 was incubated with Siah1 T156C (Figure 2d) within the experimental error. As expected, BI-117C3 was unable to covalently modify *wt* Siah1 (Figure 2e). Because Siah possesses additional solvent exposed Cys residues, this data further confirms that the mildly reactive functionality introduced in the peptide reacts only with the directed Cys residue, after proper binding takes places.

We next sought a solvent-accessible cysteine residue in the wild-type protein adjacent to the peptide-binding site to exploit in this manner. We observed that the side-chain of Cys130, conserved in Siah1 and Siah2, is located at the bottom of the P2 pocket (Figure 1 and Figure 3a). Cys130 is adjacent to, but not part of, the Zn^{2+}-binding motif of the second zinc finger domain (Figure 1). Using modeling techniques we predicted that replacement of BI-107F1 at position 123 with a lysine residue with the side chain amino group conjugated to an acrylamide group (Lys-acm, BI-107F7; Table 1), should provide a warhead of suitable length to enable thioether bond formation between wild-type Siah and BI-107F7 without disturbing other (non-covalent) interactions. Indeed, we found that BI-107F7 efficiently competed with PHYL 108-130 for binding to Siah1 (IC_{50} = 0.1 μM; Table 1).

The Siah1/BI-107F7 complex was determined at 2.4 Å resolution. We observed continuous electron density between the peptide and Cys130 of Siah1 that was fully consistent with the presence of the modified lysine side chain linked directly to the protein via a thioether bond (Figure 3b and c). MALDI-TOF mass spectrometry confirmed the formation of the covalent complex (Figures 3d and e).

Upon inspection of the Siah1/BI-107F7 crystal structure data, it became apparent that a peptide with a side-chain linker shorter by one methylene group may allow for a more optimal distance between the two reactive groups. Thus we introduced an ornithine-acm at position 123 resulting in BI-107F11 (Table 1). Indeed, BI-107F11 was about twice as effective as BI-107F7 at competing for binding to Siah1 (IC_{50} = 0.05 μM; Table 1). A peptide that combines the functionality of BI-117C3 and BI-107F11 was also synthesized and tested. BI-120G4 (IC_{50} = 0.001 μM; Table 1), with both a Dap-acm in place of Ala118 and Orn-acm in place of Thr123, was even more efficient at disrupting the PHYL-SiahT156C interaction than BI-117C3, under the same DELFIA experimental conditions.

BI-120G4 could be a useful chemical probe in the further elucidation of the Siah mechanism of action in cells that stably express Siah1 T156C. BI-107F11 and BI-107F7 although less potent, could be used in cell based assays targeting wild type Siah.

In cell, Siah targets PHD1/3 for ubiquitination and degradation, thereby destabilizing HIF-1α (Nakayama et al., 2004). Accordingly, Siah inhibition stabilizes PHD3. A cell-penetrating version of PHYL 108-130 with an N-terminal penetratin-P10 sequence (Pen-P10; Table 1) has been previously reported to antagonize Siah mediated PHD3 degradation (Moller et al., 2009). Similarly, we fused the most promising covalent peptides targeting Cys130 to either Pen-P10, for comparison with the previously reported peptide, or with a simpler cell penetrating sequence from HIV-TAT (Table 1). Adding Pen-P10 to the N-terminus of BI-107F11 resulted in BI-107G3 (Table 1). We found that BI-107G3 more efficiently reduced the level of HIF-1α in human melanoma Lu1205 cells that were maintained under hypoxia than did Pen-P10-PHYL (Figure 4a). As expected, BI-107G3 also stabilizes PHD3 more efficiently than Pen-P10-PHYL in HEK293T cells (Figure 4b). It should be noted that the cell-based system makes use of a HA-Siah and Myc-PDH3 stable expression system. As a result, the levels of both enzyme and substrate in these cells are higher than endogenous levels. This could have a large inflationary effect on the EC_{50} values obtained with this assay even when testing our covalent compounds. Notably, the dose dependent shift in HA-Siah migration (Figure 4b) may reflect covalent binding of BI-107G3 to Siah in the cellular context. These findings establish the ability of a BI-107G3, which covalently binds Siah, to attenuate Siah-mediated degradation of PHD3, with concomitant effects on HIF-1α levels. Interestingly, BI-107G3 inhibition of Siah also reduced Erk phosphorylation, suggesting that Siah effect on Sprouty2 (Nadeau et al., 2007; Qi et al., 2008), a negative regulator of Ras/Raf signaling, was also attenuated. Thus we conclude that BI-107G3 represents an efficient covalent inhibitor of Siah cellular activity.

To further address the specificity of the peptides in inhibiting Siah in vitro and in cell, we tested the HIV-TAT cell penetrating version of BI-107F7, namely BI-107F9, (Table 1) and its scrambled equivalent, BI-107F8 (Table 1). Similar to what was previously observed for PHYL (Moller et al., 2009), BI-107F7 was not effective in inhibiting Siah auto-ubiquitination in vitro (Figure 5a). However, both BI-107F7 and its cell penetrating derivative BI-107F9 were efficient at inhibiting Siah2-directed ubiquitination of substrate OGDH (Figure 5b). Similarly, in cell we found that addition of BI-107F9 (but not the control scrambled peptide BI-107F8) attenuated Siah2 degradation of exogenously expressed PHD3 (Figure 5c). Finally, BI-107F9 effectively reduced the level of HIF-1α in mouse melanoma SW1 cells that were maintained under hypoxia (Figure 5d). These observations further substantiate the selectivity of the observed effects of the covalent peptides on the inhibition of the PHD3-HIF-1α axis and therefore on the hypoxia response in several cell lines. These findings establish the ability of the reported covalent Siah peptides to inhibit Siah-mediated degradation of PHD3 and other substrates.

Significance

In conclusion, we have used a structure-based approach to derive novel covalent peptide-based inhibitors of Siah that are potentially orders of magnitude more effective than parent peptides. These molecules could serve as chemical probes to further assess the role of Siah in tumorigenesis as well as to validate this complex ubiquitin ligase as a target for novel anti-cancer therapies. Moreover, our data suggest that the introduction of a mildly reactive Michael-acceptor in peptides of moderate affinity may represent a novel route for the optimization of these molecules into more effective peptide-based therapeutics.

Experimental Procedures

Chemistry

Fmoc-Dap(acryl amide)-OH was prepared and used as a building block for the synthesis of desired peptide in solid phase synthesis. Fmoc-Dap-OH was acrylated with acryl chloride in the presence of aqueous sodium carbonate in 1,4-dioxane to give the desired building block in 90% purity (see supplementary information and Figure S1). Similarly, Fmoc-Orn(acryl amide)-OH and Fmoc-Lys(acryl amide)-OH were prepared. Alternatively, some peptide containing acryl amides were synthesized using Dde as protecting group on Dap, Orn, and Lys in their side chain, after completion of peptide sequence on the resin, Dde group was selectively removed by the treatment of 2% hydrazine in DMF, followed by addition of acryl acid using standard peptide coupling conditions. Resin and all other protecting groups were removed using TFA. All final compounds were purified by HPLC using acetonitrile-water system. The detailed experimental procedures for compounds synthesis, purification and characterization are provided as supplementary information (Figures S1 and S2).

Protein expression and purification

Siah1 81-282 and Siah1 81-282 (T156C) were subcloned into pET15b (Novagen) and expressed as previously described (Santelli et al., 2005). Siah1 81-282 (T156C) was constructed using QuikChange™ site-directed mutagenesis (Stratagene) using Siah1 81-282 as a template.

DELFIA Assay (dissociation enhanced lanthanide fluoro-immuno assay)

To each well of 96-well streptavidin-coated plates (Perkin-Elmer) 100 μL of a 100 ng/ml solution of biotin-PHYL (biotin-lc-QQERTKLRPVAMVRPTVRVQPQL, where lc indicates a hydrocarbon chain of 6 methylene groups) was added. After 1 h incubation and elimination of unbound biotin-PHYL by three washing steps, 87 μL of Eu-labeled anti-his6

antibody solution (300 ng/ml; 1.9 nM), 2.5 μL DMSO solution containing test compound, and 10 μL solution of his6-Siah1 (aa 81-282) or his_6-Siah1 T156C (aa 81-282) for a final protein concentration of 100 nM was added. After 1 h incubation at 0°C, each well was washed five times to eliminate unbound protein and the Eu-antibody if displaced by a test compound. Subsequently, 200 μL of enhancement solution (Perkin-Elmer) was added to each well and fluorescence measured after 10 min incubation (excitation wavelength, 340 nm; emission wavelength, 615 nm). Controls include unlabeled peptide and blanks receiving no compounds. Protein and peptide solutions were prepared in DELFIA buffer (Perkin-Elmer).

Mass Spectrometry Analysis

Molecular weight analysis was done using an Autoflex II MALDI TOF/TOF (Bruker Daltonics). The reaction buffer (0.5x PBS) was used as a control to compare against the spectra from protein incubated with peptide. For MS analysis, equal volume (2 μl) of each sample and MALDI Matrix solution (sinapic acid; 20 mg/ml in 50% acetonitrile-0.1% trifluoroacetic acid solution) were co-crystallized on the MALDI target plate and allowed to air dry for 5 min. Mass spectra were acquired and processed with FlexAnalysis 2.4. The overlay protein molecular weight spectra against background buffer as well as control protein and peptide conjugated is shown. The protein mass shift correlating to peptide molecular weight was observed in conjugated sample. The data was further processed using the FlexAnalysis peak picking method (using the Centroid mass find routine, with a signal to noise threshold of 5, maximum number of peaks set to 50, a peak width of 40 m/z and height at 80% as well as Top Hat baseline subtraction). The data reveals that under these conditions a mass difference between replicates is about 70 Da (as in Figure 3) or lower (as in Figure 2); these small deviations are within Bruker Daltonics Manufacturer standards for a protein of 23 kDa. A mass shift corresponding to Na+ and Ca+ is also observed additional to the mass of the peptides.

X-ray crystallography—Siah1 81-282 (wild-type and T156C mutant) for crystallographic studies was purified as described (Santelli et al., 2005). To crystallize the Siah1/E1 complex by the sitting drop vapor diffusion method, Siah1 at 6 mg/ml was mixed with a 2.5-fold excess of BI-107E1 and mixed with an equal amount of reservoir solution made of 10% polyethyleneglycol (PEG) 6000, 5% 2-Methyl-2,4-pentanediol (MPD), 100 mM 4-(2-hydroxyethyl)-1-piperazineethanesulfonic acid (HEPES) pH 6.5. 20% glycerol with 10% MPD was used as cryoprotectant for data collection at beamline 9–2 at Stanford Synchrotron Radiation Lightsource (SSRL). Data were reduced using HKL2000(Minor et al., 2000) (Table 2). The structure was solved by molecular replacement with the program Phaser (McCoy et al., 2007) using residues 161–282 of chain A of the Siah1-SIP complex (Santelli et al., 2005) (pdb code 2a25) followed by manual fitting of the Zinc-finger domains and the peptide, model building in Coot (Emsley and Cowtan, 2004) and refinement with Refmac5 (Murshudov et al., 1997) without imposing non-crystallographic symmetry (ncs) constraints. The asymmetric unit (ASU) contains one Siah1 dimer and one copy of BI-107E1 per Siah1 subunit. Refinement parameters are reported in Table 2. The complex between Siah1 and BI-107F7 was obtained by mixing the protein with a 2-fold excess peptide and incubating at 4 °C for 16–18 h. Thanks to the net positive charge on the peptide, the $Siah_2F7_2$ species was separated from $Siah1_2F7$ and $Siah1_2$ by anion exchange. Virtually all of the peptide in the recovered complex was covalently bound to the protein as judged by SDS PAGE. Crystals were obtained by the sitting drop vapor diffusion method using 60–65% MPD, 100 mM N,N-Bis(2-hydroxyethyl)glycine pH 9.0 as the reservoir solution. Data were collected at SSRL beamline 12–2 and reduced with HKL2000 (Minor et al., 2000). The structure was solved by molecular replacement and refined as done with the Siah1/E1 complex. Continuous density connecting the peptide to Cys130 was visible from the early stages of

refinement. The ASU contains one Siah1 dimer (residues 92–282) and all 13 amino-acids of each copy of BI-107F7, 118 water and one MPD molecule. The $[Siah1(T156C)]_2C3_2$ complex was purified and crystallized as described for $Siah_2F7_2$, a dataset was collected at SSRL beamline 9-2 and reduced with imosflm (Leslie and Powell, 2007). A refined $Siah_2F7_2$ dimer was used as search model for molecular replacement. The final model contains one Siah1 dimer covalently bound to two peptide molecules. All three refined models with BI-107E1, BI-107F7 and BI-117C3 contain no residues in outlier regions of the Ramachandran plot as assessed with rampage (Lovell et al., 2002) with 97.9%, 98.4% and 97.2% of residues respectively in the most favored regions.

Cell culture

Lu1205, SW1 and HEK293T cells were cultured in Dulbecco's modified Eagle's medium (Thermo Scientific) supplemented with 10% fetal bovine serum and antibiotics. Cell cultures were maintained at 37°C in 5% CO_2.

Plasmid and transfection

The Flag-OGDH, HA-Siah2, Myc-PHD3 and GST-Siah2 plasmids have been described previously (Habelhah et al., 2004; Scortegagna et al., 2011). GST-siah2 was expressed in *E. coli* BL21 and purified using immobilized glutathione-Sepharose beads (Thermo Scientific) as described previously (Habelhah et al., 2004). HEK293T cells were transfected using the jetPRIME DNA transfection reagent kit (Polyplus, France) according to the manufacture's protocol. In all cases, the total amount of DNA was normalized by the addition of empty control plasmids.

In vitro ubiquitination assay

Flag-OGDH protein was obtained from HEK293T cells transfected with FLAG-OGDH. After transfection for 24 h, cells are harvested and lysed in IP buffer containing 50 mM Tris-HCl, pH 7.4, 150 mM NaCl, 1% Triton-X, 1 mM EDTA, 1 mM PMSF, 10 μg/ml aprotinin, 10 μg/ml leupeptin, and 1 μg/ml pepstatin A for 30 min at 4°C. After centrifugation at 13,000 × g for 30 min at 4°C, cell lysate (1mg protein) was incubated with 1 μg of mouse anti-Flag antibody (Sigma) 2 h and further incubated for 2 h with 20 μl of protein A/G PLUS-agarose beads (Santa Cruz). The beads were washed three times with the same lysis buffer and one time with ubiquitination assay buffer (50 mM Tris-HCl, pH 8.0, 5 mM $MgCl_2$, 0.5 mM dithiothreitol, 2 mM NaF, and 2 mM ATP). Immunoprecipitated Flag-OGDH was subjected to an in vitro ubiquitination assay (20 μl) in ubiquitination buffer supplemented with purified GST-Siah2 (1 μg), HA-Ub (1 μg), E1 (UBE1, 50 μg), E2 (UbcH5c, 250 ng) (HA-Ub, E1, and E2 are from Boston Biochem, Cambridge, MA) and different amount of Siah peptide inhibitors for 45 min at 37°C. The reaction mixtures were washed four times, before being eluted in Laemmli buffer, and separated on 8% SDS-PAGE followed by Western blot analysis with anti-Flag antibody. The same ubiquitination reactions were performed to determine the effect of Siah peptide inhibitors on Siah self ubiquitination in the absence of Flag-OGDH in the reaction mixtures. After 45 min at 37°C, the reaction mixtures were mixed with Laemmli buffer, heated and subjected to 8% SDS-PAGE directly followed by Western blot analysis with anti-HA antibody. The same membrane was striped and re-probed with anti-GST antibody.

Protein preparation and Western blotting

HEK293T cells were transfected with Flag-OGDH or Myc-PHD3, along with or without HA-Siah2 for 16 h. Different amounts of different Siah peptide inhibitors were added to cells and further incubated for 6 h. Cells were then washed with cold PBS and lysed in lysis buffer (50 mM Tris-HCl, pH 7.4, 150 mM NaCl, 1% NP-40, 1 mM EDTA, 10 μg/ml

aprotinin, 1 μg/ml pepstatin A, 10 μg/ml leupeptin, 2 mM phenylmethylsulfonyl fluoride, 20 μM microcystin-LR, 2.5 mM sodium orthovanadate) for 30 minutes on ice. Cell lysates were obtained by centrifugation at 13,000 × g for 30 min at 4°C. The protein concentration was determined using Bio-Rad protein assay solution. Equal amounts of cell lysate (50 μg) were resolved by SDS-PAGE and transferred to polyvinylidene difluoride membranes (PerkinElmer Life Sciences, Waltham, MA). Membranes were blocked with 5% BSA/PBST for 1 h and incubated with primary antibodies (mouse anti-Flag antibody, Sigma, 1:1000; mouse anti-Myc antibody, Santa Cruz, 1:1000; rabbit anti-HA antibody, Santa Cruz, 1:1000; mouse anti-tubulin antibody, Santa Cruz, 1:1000) for 1 h at room temperature or overnight at 4°C with shaking. Following three times wash with PBST (PBS containing Tween 20, 0.05% v/v), membranes were incubated with second antibody for 1 h at room temperature. Bound antibodies were detected with horseradish peroxidase-conjugated anti-rabbit antibody (Cell Signaling) for polyclonal antibodies or horseradish peroxidase-conjugated anti-mouse antibody (Cell Signaling) for monoclonal antibodies followed by enhanced chemiluminescence using Western Lightning reagent (PerkinElmer Life Sciences).

Hypoxia Treatment

Half million Lu1205 cells were plated in 6-well plate and allowed to attach overnight. Different amounts of different penetrating Siah peptide inhibitors were added to cells. Cells were exposed to hypoxia (1%) for 6 h and lysed immediately on ice as described above. Cell lysates were subjected to Western blot analysis as described above with rabbit anti-HIF-1α antibody (a gift from Dr. Gary Chiang, 1:1000). The same membrane was striped and probed again with mouse anti-tubulin antibody.

Supplementary Material

Refer to Web version on PubMed Central for supplementary material.

References

Ahmed AU, Schmidt RL, Park CH, Reed NR, Hesse SE, Thomas CF, Molina JR, Deschamps C, Yang P, Aubry MC, Tang AH. Effect of disrupting seven-in-absentia homolog 2 function on lung cancer cell growth. J Natl Cancer Inst. 2008; 100:1606–1629. [PubMed: 19001609]

Avraham E, Szargel R, Eyal A, Rott R, Engelender S. Glycogen synthase kinase 3beta modulates synphilin-1 ubiquitylation and cellular inclusion formation by SIAH: implications for proteasomal function and Lewy body formation. J Biol Chem. 2005; 280:42877–42886. [PubMed: 16174773]

Bedogni B, Powell MB. Hypoxia, melanocytes and melanoma - survival and tumor development in the permissive microenvironment of the skin. Pigment Cell Melanoma Res. 2009; 22:166–174. [PubMed: 19222803]

Boulton SJ, Brook A, Staehling-Hampton K, Heitzler P, Dyson N. A role for Ebi in neuronal cell cycle control. EMBO J. 2000; 19:5376–5386. [PubMed: 11032805]

Bruzzoni-Giovanelli H, Faille A, Linares-Cruz G, Nemani M, Le Deist F, Germani A, Chassoux D, Millot G, Roperch JP, Amson R, et al. SIAH-1 inhibits cell growth by altering the mitotic process. Oncogene. 1999; 18:7101–7109. [PubMed: 10597311]

Confalonieri S, Quarto M, Goisis G, Nuciforo P, Donzelli M, Jodice G, Pelosi G, Viale G, Pece S, Di Fiore PP. Alterations of ubiquitin ligases in human cancer and their association with the natural history of the tumor. Oncogene. 2009; 28:2959–2968. [PubMed: 19543318]

Davies H, Bignell GR, Cox C, Stephens P, Edkins S, Clegg S, Teague J, Woffendin H, Garnett MJ, Bottomley W, et al. Mutations of the BRAF gene in human cancer. Nature. 2002; 417:949–954. [PubMed: 12068308]

Della NG, Senior PV, Bowtell DD. Isolation and characterisation of murine homologues of the Drosophila seven in absentia gene (sina). Development. 1993; 117:1333–1343. [PubMed: 8404535]

Dong X, Tsuda L, Zavitz KH, Lin M, Li S, Carthew RW, Zipursky SL. ebi regulates epidermal growth factor receptor signaling pathways in Drosophila. Genes Dev. 1999; 13:954–965. [PubMed: 10215623]

Emsley P, Cowtan K. Coot: model-building tools for molecular graphics. Acta Crystallogr D Biol Crystallogr. 2004; 60:2126–2132. [PubMed: 15572765]

Fernandez-Medarde A, Santos E. Ras in cancer and developmental diseases. Genes & cancer. 2011; 2:344–358. [PubMed: 21779504]

Frasor J, Danes JM, Funk CC, Katzenellenbogen BS. Estrogen down-regulation of the corepressor N-CoR: mechanism and implications for estrogen derepression of N-CoR-regulated genes. Proc Natl Acad Sci U S A. 2005; 102:13153–13157. [PubMed: 16141343]

Habelhah H, Frew IJ, Laine A, Janes PW, Relaix F, Sassoon D, Bowtell DD, Ronai Z. Stress-induced decrease in TRAF2 stability is mediated by Siah2. EMBO J. 2002; 21:5756–5765. [PubMed: 12411493]

Habelhah H, Laine A, Erdjument-Bromage H, Tempst P, Gershwin ME, Bowtell DD, Ronai Z. Regulation of 2-oxoglutarate (alpha-ketoglutarate) dehydrogenase stability by the RING finger ubiquitin ligase Siah. J Biol Chem. 2004; 279:53782–53788. [PubMed: 15466852]

House CM, Frew IJ, Huang HL, Wiche G, Traficante N, Nice E, Catimel B, Bowtell DD. A binding motif for Siah ubiquitin ligase. Proc Natl Acad Sci U S A. 2003; 100:3101–3106. [PubMed: 12626763]

House CM, Hancock NC, Moller A, Cromer BA, Fedorov V, Bowtell DD, Parker MW, Polekhina G. Elucidation of the substrate binding site of Siah ubiquitin ligase. Structure. 2006; 14:695–701. [PubMed: 16615911]

House CM, Moller A, Bowtell DD. Siah proteins: novel drug targets in the Ras and hypoxia pathways. Cancer Res. 2009; 69:8835–8838. [PubMed: 19920190]

Leslie, AGW.; Powell, HR. Evolving Methods for Macromolecular Crystallography. 2007. p. 41-51.

Li S, Li Y, Carthew RW, Lai ZC. Photoreceptor cell differentiation requires regulated proteolysis of the transcriptional repressor Tramtrack. Cell. 1997; 90:469–478. [PubMed: 9267027]

Liani E, Eyal A, Avraham E, Shemer R, Szargel R, Berg D, Bornemann A, Riess O, Ross CA, Rott R, Engelender S. Ubiquitylation of synphilin-1 and alpha-synuclein by SIAH and its presence in cellular inclusions and Lewy bodies imply a role in Parkinson's disease. Proc Natl Acad Sci U S A. 2004; 101:5500–5505. [PubMed: 15064394]

Lovell SC, Davis IW, Arendall WB III, de Bakker PIW, Word JM, Prisant MG, Richardson JS, Richardson DC. Structure validation by Cα geometry: φ/ψ and Cβ deviation. Proteins: Structure, Function & Genetics. 2002:437–450.

Maly DJ, Allen JA, Shokat KM. A mechanism-based cross-linker for the identification of kinase-substrate pairs. J Am Chem Soc. 2004; 126:9160–9161. [PubMed: 15281787]

Matsuzawa SI, Reed JC. Siah-1, SIP, and Ebi collaborate in a novel pathway for beta-catenin degradation linked to p53 responses. Mol Cell. 2001; 7:915–926. [PubMed: 11389839]

McCoy AJ, Grosse-Kunstleve RW, Adams PD, Winn MD, Storoni LC, Read RJ. Phaser crystallographic software. J Appl Crystallogr. 2007; 40:658–674. [PubMed: 19461840]

Minor W, Tomchick D, Otwinowski Z. Strategies for macromolecular synchrotron crystallography. Structure. 2000; 8:R105–110. [PubMed: 10801499]

Moller A, House CM, Wong CS, Scanlon DB, Liu MC, Ronai Z, Bowtell DD. Inhibition of Siah ubiquitin ligase function. Oncogene. 2009; 28:289–296. [PubMed: 18850011]

Murshudov GN, Vagin AA, Dodson EJ. Refinement of macromolecular structures by the maximum-likelihood method. Acta Crystallogr D Biol Crystallogr. 1997; 53:240–255. [PubMed: 15299926]

Nadeau RJ, Toher JL, Yang X, Kovalenko D, Friesel R. Regulation of Sprouty2 stability by mammalian Seven-in-Absentia homolog 2. J Cell Biochem. 2007; 100:151–160. [PubMed: 16888801]

Nagano Y, Yamashita H, Takahashi T, Kishida S, Nakamura T, Iseki E, Hattori N, Mizuno Y, Kikuchi A, Matsumoto M. Siah-1 facilitates ubiquitination and degradation of synphilin-1. J Biol Chem. 2003; 278:51504–51514. [PubMed: 14506261]

Nakayama K, Frew IJ, Hagensen M, Skals M, Habelhah H, Bhoumik A, Kadoya T, Erdjument-Bromage H, Tempst P, Frappell PB, et al. Siah2 regulates stability of prolyl-hydroxylases, controls

HIF1alpha abundance, and modulates physiological responses to hypoxia. Cell. 2004; 117:941–952. [PubMed: 15210114]

Nakayama K, Qi J, Ronai Z. The ubiquitin ligase Siah2 and the hypoxia response. Mol Cancer Res. 2009; 7:443–451. [PubMed: 19372575]

Qi J, Nakayama K, Cardiff RD, Borowsky AD, Kaul K, Williams R, Krajewski S, Mercola D, Carpenter PM, Bowtell D, Ronai ZA. Siah2-dependent concerted activity of HIF and FoxA2 regulates formation of neuroendocrine phenotype and neuroendocrine prostate tumors. Cancer Cell. 2010a; 18:23–38. [PubMed: 20609350]

Qi J, Nakayama K, Gaitonde S, Goydos JS, Krajewski S, Eroshkin A, Bar-Sagi D, Bowtell D, Ronai Z. The ubiquitin ligase Siah2 regulates tumorigenesis and metastasis by HIF-dependent and -independent pathways. Proc Natl Acad Sci U S A. 2008; 105:16713–16718. [PubMed: 18946040]

Qi J, Pellecchia M, Ronai ZA. The Siah2-HIF-FoxA2 axis in prostate cancer - new markers and therapeutic opportunities. Oncotarget. 2010b; 1:379–385. [PubMed: 21037926]

Roperch JP, Lethrone F, Prieur S, Piouffre L, Israeli D, Tuynder M, Nemani M, Pasturaud P, Gendron MC, Dausset J, et al. SIAH-1 promotes apoptosis and tumor suppression through a network involving the regulation of protein folding, unfolding, and trafficking: identification of common effectors with p53 and p21(Waf1). Proc Natl Acad Sci U S A. 1999; 96:8070–8073. [PubMed: 10393949]

Santelli E, Leone M, Li C, Fukushima T, Preece NE, Olson AJ, Ely KR, Reed JC, Pellecchia M, Liddington RC, Matsuzawa S. Structural analysis of Siah1-Siah-interacting protein interactions and insights into the assembly of an E3 ligase multiprotein complex. J Biol Chem. 2005; 280:34278–34287. [PubMed: 16085652]

Schmidt RL, Park CH, Ahmed AU, Gundelach JH, Reed NR, Cheng S, Knudsen BE, Tang AH. Inhibition of RAS-mediated transformation and tumorigenesis by targeting the downstream E3 ubiquitin ligase seven in absentia homologue. Cancer Res. 2007; 67:11798–11810. [PubMed: 18089810]

Scortegagna M, Subtil T, Qi J, Kim H, Zhao W, Gu W, Kluger H, Ronai ZA. USP13 enzyme regulates Siah2 ligase stability and activity via noncatalytic ubiquitin-binding domains. J Biol Chem. 2011; 286:27333–27341. [PubMed: 21659512]

Semenza GL. Defining the role of hypoxia-inducible factor 1 in cancer biology and therapeutics. Oncogene. 2010; 29:625–634. [PubMed: 19946328]

Shah M, Stebbins JL, Dewing A, Qi J, Pellecchia M, Ronai ZA. Inhibition of Siah2 ubiquitin ligase by vitamin K3 (menadione) attenuates hypoxia and MAPK signaling and blocks melanoma tumorigenesis. Pigment Cell Melanoma Res. 2009; 22:799–808. [PubMed: 19712206]

Singh J, Petter RC, Baillie TA, Whitty A. The resurgence of covalent drugs. Nat Rev Drug Discov. 2011; 10:307–317. [PubMed: 21455239]

Szargel R, Rott R, Eyal A, Haskin J, Shani V, Balan L, Wolosker H, Engelender S. Synphilin-1A inhibits seven in absentia homolog (SIAH) and modulates alpha-synuclein monoubiquitylation and inclusion formation. J Biol Chem. 2009; 284:11706–11716. [PubMed: 19224863]

Tang AH, Neufeld TP, Kwan E, Rubin GM. PHYL acts to down-regulate TTK88, a transcriptional repressor of neuronal cell fates, by a SINA-dependent mechanism. Cell. 1997; 90:459–467. [PubMed: 9267026]

Winter M, Sombroek D, Dauth I, Moehlenbrink J, Scheuermann K, Crone J, Hofmann TG. Control of HIPK2 stability by ubiquitin ligase Siah-1 and checkpoint kinases ATM and ATR. Nat Cell Biol. 2008; 10:812–824. [PubMed: 18536714]

Xu Z, Sproul A, Wang W, Kukekov N, Greene LA. Siah1 interacts with the scaffold protein POSH to promote JNK activation and apoptosis. J Biol Chem. 2006; 281:303–312. [PubMed: 16230351]

Zhang J, Guenther MG, Carthew RW, Lazar MA. Proteasomal regulation of nuclear receptor corepressor-mediated repression. Genes Dev. 1998; 12:1775–1780. [PubMed: 9637679]

Highlights

- Inhibition of ubiquitin ligases, such as Siah, is very challenging;
- Siah docking site was targeted using a structure-based approach;
- Careful design of peptide mimetics with a Cys-trapping moiety;
- The work resulted in potent and effective covalent inhibitors of Siah.

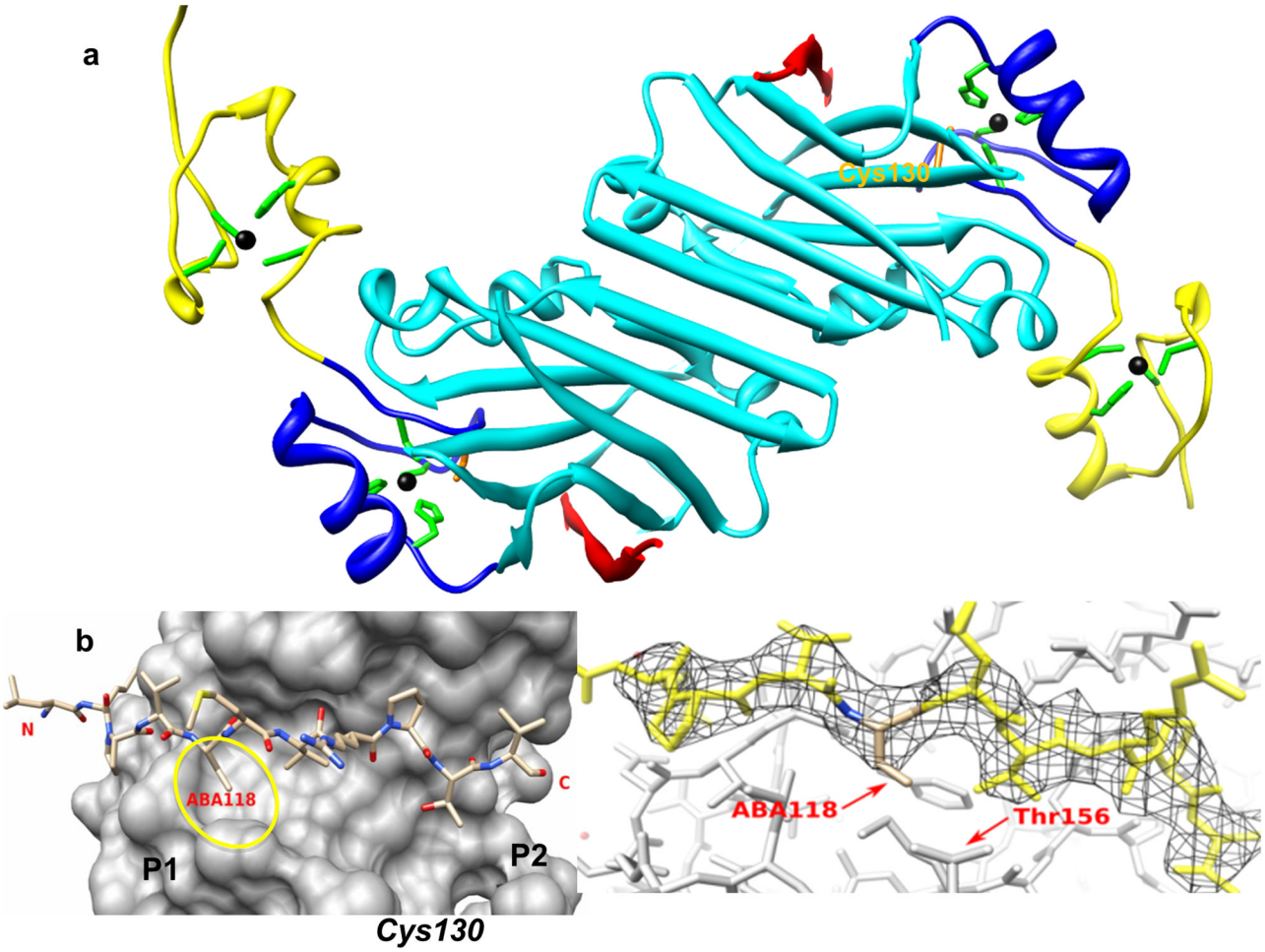

Figure 1. X-ray structure of Siah1 in complex with BI-107E1

a) Ribbon representation of Siah1-ΔRING in complex with BI-107E1. The PHYL binding domain is depicted in cyan, the two Zn-fingers in yellow and blue, respectively. Zn ions (black) and their coordinating residues (green stick models) are displayed, while the side chain of Cys130 is labeled and displayed in orange. BI-107E1 (red) assumes an extended conformation and participates in a β-sheet formation with Siah1. **b)** Detail of the binding mode of BI-107E1 (stick representation) on the surface of Siah1. Aba118 indicates the ethyl-glycine residue at position 118 of the peptide (Table 1). The two hydrophobic P1 and P2 sub-pockets used in our optimization strategies as well as the location of Cys130 are schematically indicated. **c)** BI-107E1 in its 2fo-fc electron density map contoured at 1.2 σ. The proximity of peptide residue 118 and protein residue Thr156 are highlighted.

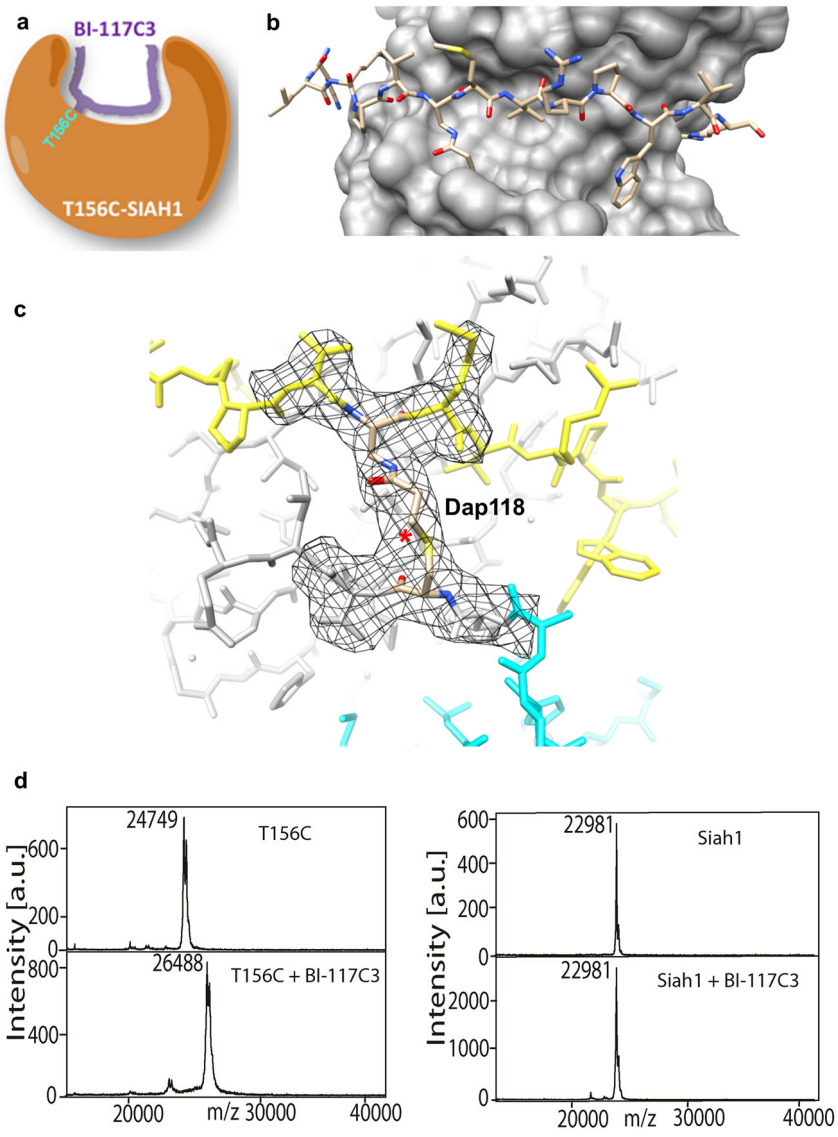

Figure 2. Structural characterization of Siah1-T156C in complex with BI-117C3

a) Schematic representation of the peptide-Siah covalent complex. **b**) View of BI-117C3 (stick representation) bound to Siah-T156C (surface). Although two alternative conformations were modeled for Dap-acrylamide at position 118 and Trp123 of the peptide and for Siah1 Cys156 in the Siah1/BI-117C3 complex, only one is shown here for clarity. See also Figures S1 and S2 regarding the chemical structure of BI-117C3 and its synthesis. **c)** Close-up view of the covalent bonds formed between BI-117C3 and Siah1 T156C shown in its 2fo-fc electron density maps contoured at 1.2 σ. The newly formed bond is marked with the asterisk. Dap118 indicates the Dap-acrylamide residue introduced at position 118 of the peptide (Table 1). Only the electron density around residues close to the reacting groups is shown. **d)** and **e)** MALDI-TOF MS spectra of Siah1 in presence of BI-117C3. The spectra of wt-Siah1 in absence and presence of 117C3 are reported in **e**, while the spectra of Siah1-T156C in absence and presence of the same peptide are reported in **d**. Note that the molecular weight of Siah1-T156C (panel d) is larger than that of wt-Siah1 (panel e) because the latter lacks the 6His-tag.

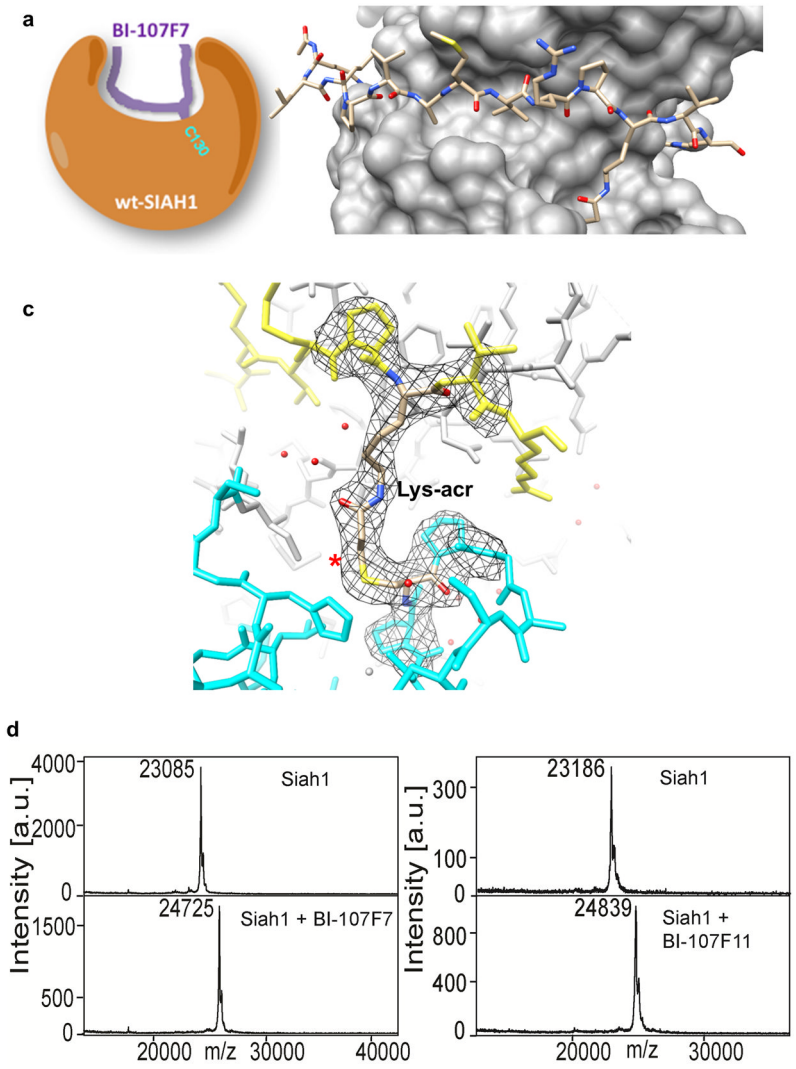

Figure 3. Structural characterization of wt-Siah1 in complex with BI-107F7

a) Schematic representation of the peptide-Siah covalent complex. **b**) View of BI-107F7 (stick representation) bound to wt-Siah (surface), reported in the same orientation as in Figure 2. **c)** Close-up view of the covalent bonds formed between BI-107F7 and wt-Siah1 shown in its 2fo-fc electron density maps contoured at 1.2 σ. The newly formed bond is marked with the asterisk. Lys-acr refers to the Lysine-acrylamide residue introduced at position 123 of the peptide (Table 1). Only the electron density around residues close to the reacting groups is shown. **d** and **e**) MALDI-TOF MS spectra of wt-Siah1 collected in absence and presence of BI-107F7 and BI-107F11, respectively.

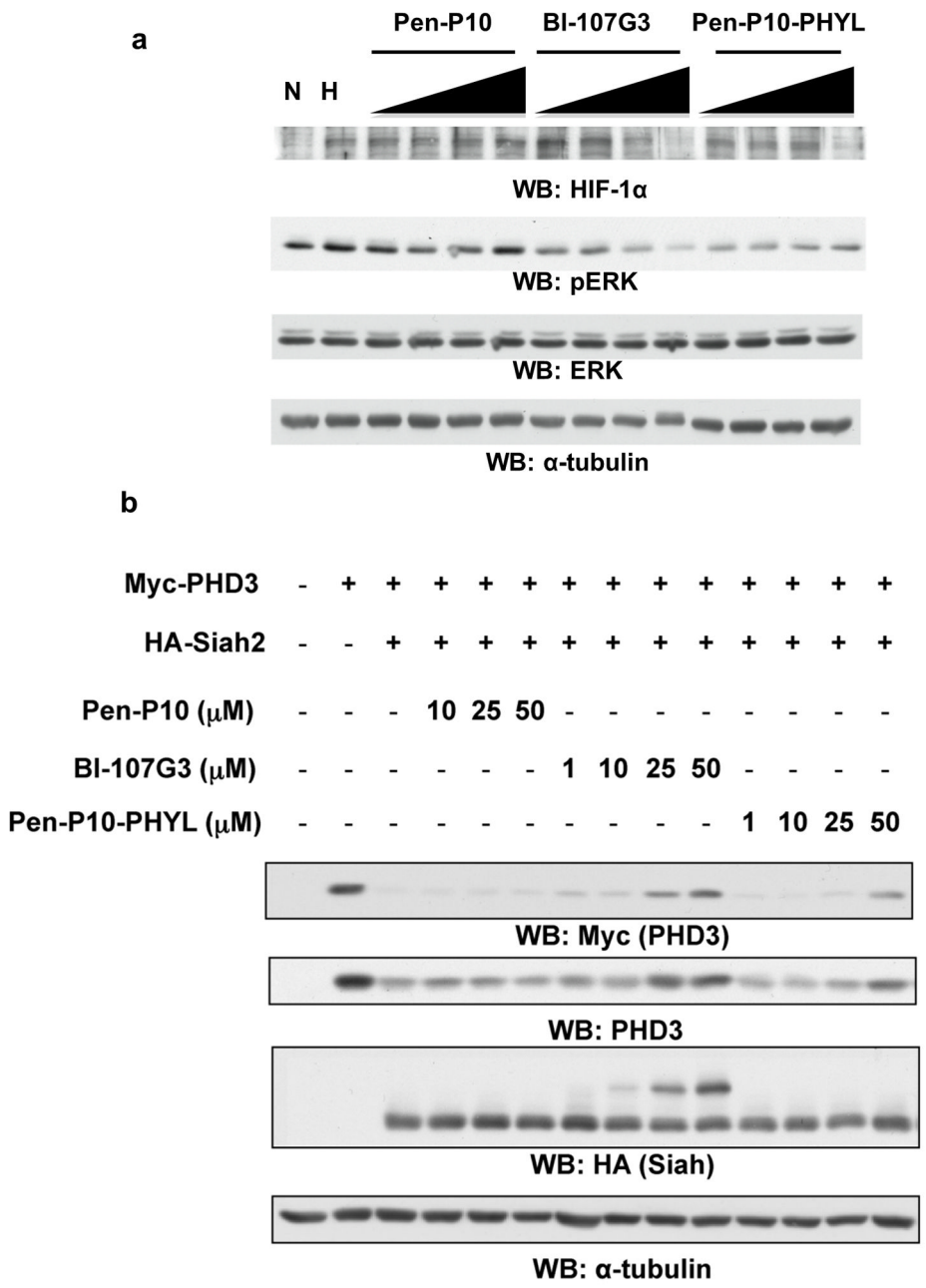

Figure 4. BI-107G3 is more efficient at stabilizing PHD3 than Pen-P10-PHYL

a) Cell-permeable synthetic PHYL peptide inhibits HIF-1α stabilization during hypoxia. LU1205 cells were treated with increasing amounts of compound in DMEM (no serum) for 2 hours under normoxia or hypoxia (2% oxygen in hypoxia workstation). The varied compound concentrations 1, 10, 25, and 50 μM. Control peptides used are Pen-P10-PHYL and Pen-P10 alone (Table 1). Blots were probed for endogenous HIF-1α and phospho-Erk. Even loading was confirmed with α-tubulin antibodies. **b)** To compare the inhibitory effects of BI-107G3 with that of Pen-P10-PHYL and Pen-P10 alone, HEK293T cells were transfected with Myc-PHD3 and HA-Siah2 and then treated with 1, 10, 25, and 50 μM of the corresponding peptide. Cells were lysed 24 hours later and analyzed by Western blotting

with FMyc, PHD3, and HA antibodies. Even loading was confirmed with α-tubulin antibodies.

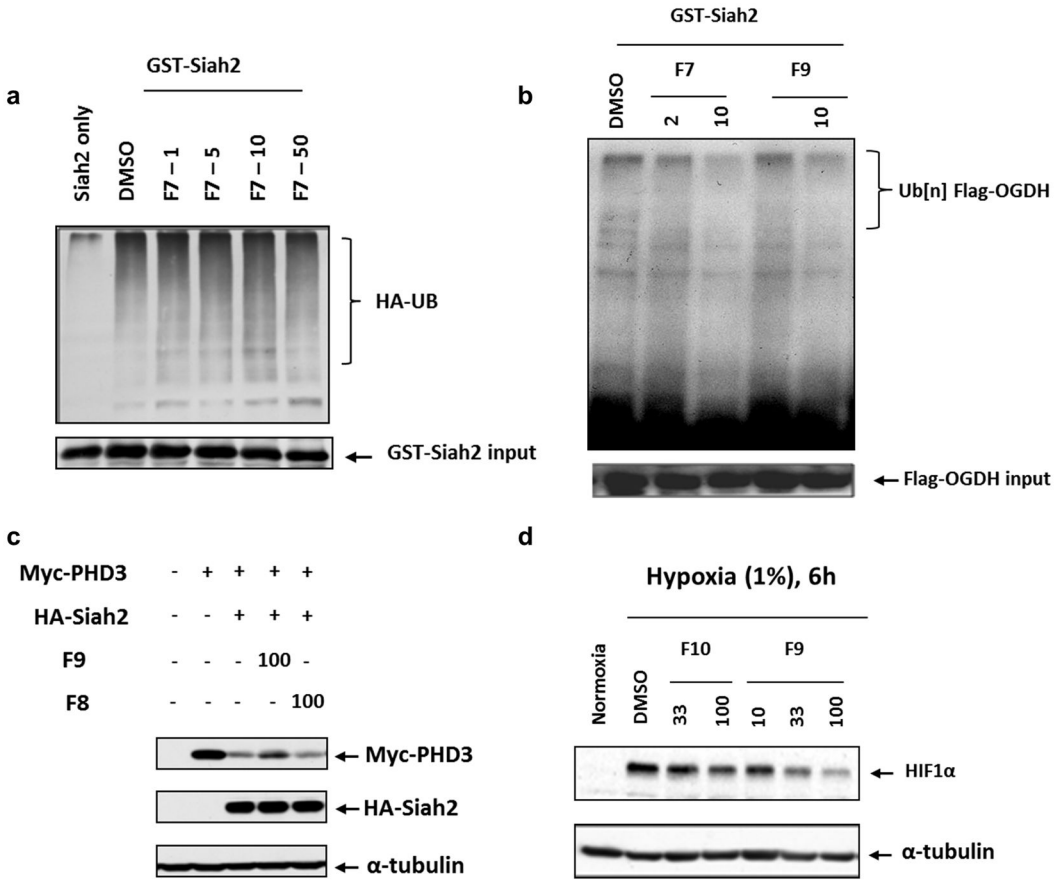

Figure 5. Effect of Siah2 inhibitory peptides on Siah2 ubiquitination and activity in vitro and in cell

a) In vitro self-ubiquitination of Siah2 was performed in the presence of DMSO (control) or indicated concentrations of BI-107F7 (indicated as F7), with UB-HA and ubiquitination reaction buffer. Degree of ubiquitination was monitored using antibodies to HA. **b)** In vitro ubiquitination of OGDH was monitored in the presence of indicated concentrations of BI-107F7 or BI-107F9 (indicated as F7 and F9, respectively). Poly-ubiquitinated OGDH is marked on the right panel. **c**) BI-107F9 and BI-107F8 peptides were added to SW1 melanoma cells grown in culture, and the effect of Siah2 on exogenously expressed PHD3 was monitored. α-tubulin was monitored as a loading control. **d**) BI-107F9 and BI-107F10, at the indicated concentrations, were added to cultured melanoma cells maintained in 1% O_2. 6h later cells were harvested and level of HIF-1α and α-tubulin were assessed.

Table 1

Peptide sequences, molecular weights, and IC_{50} values relative to the ability of each molecule to displace biotin-PHYL in a DELFIA assay against wild type or mutant T156C Siah. See also supplementary Table S1 for additional peptides synthesized and tested in the same assays and supplementary Figures S1 and S2 with chemical structures and synthetic schemes. Cell penetrating sequences are reported in italics.

			WT	T156C
I.D.	**Sequence**	**M.W.**	**DELFIA IC_{50} (μM)**	**DELFIA IC_{50} (μM)**
PHYL	**Ac-^{108}QQERTKLRPVAMVRPTVRVQPQL^{130}-NH_2**	2772	0.5	ND
BI-107D1	**Ac-KLRPVAMVRPTVR-NH_2**	1564	1	1
BI-107E12	**Ac-KLRPVAMVRPMVR-NH_2**	1594	1.3	0.9
BI-107F1	**Ac-KLRPVAMVRPWVR-NH_2**	1649	0.6	0.4
BI-107E1	**Ac-KLRPVɐMVRPTVR-NH_2**	1664	2	2
BI-117C3	**Ac-KLRPVδMVRPWVR-NH_2**	1761	> 100	0.006
BI-107F7	**Ac-KLRPVAMVRPαVR-NH_2**	1548	0.1	ND
BI-107F11	**Ac-KLRPVAMVRPβVR-NH_2**	1632	0.05	ND
BI-120G4	**Ac-KLRPVδMVRPβVR-NH_2**	1677	> 100	0.001
PEN-P10	***Ac-RQIKIWFQNRRMKWKKPPPPPPPPPP-NH_2***	3259	ND	ND
PEN-P10-PHYL	***Ac-RQIKIWFQNRRMKWKKPPPPPPPPPP*** **QQERTKLRPVAMVRPTVRVQPQL-NH_2**	5972	1.0	ND
BI-107G3	***Ac-RQIKIWFQNRRMKWKKPPPPPPPPPP*** **KLRPVAMVRPβVR-NH_2**	4831	0.05	ND
BI-107F9	***Ac-GRKKRRQRRRPQ*****KLRPVAMVRPαVR-NH_2**	3250	0.1	ND
BI-107F8	***Ac-GRKKRRQRRRPQ*****PMRAαPRVTVRLK-NH_2**	3250	> 100	ND
BI-107F10 (HIV-TAT)	***Ac-GRKKRRQRRRPQ-NH_2***	1663	> 100	ND

ɐ=Ethylglycine; δ=DAP-acrylamide; α=Lys-acrylamide; β=Orn-acrylamide; Ac=acetyl; ND=not determined.

Table 2
Data collection and refinement statistics

Values in parentheses are for highest-resolution shell.

	BI-107E1	BI-107F7	BI-117C3
Data collection			
Space group	$P2_1$	I23	I23
Cell parameters			
a, *b*, *c* (Å)	39.82, 87.94, 59.90	160.98	164.23
α, β, γ (°)	90, 100.6, 90		
Resolution (Å)	50–3.0 (3.11-3.00)	120–2.4 (2.44-2.40)	30–2.8 (2.95-2.80)
R_{merge}	0.077 (0.60)	0.073 (0.662)	0.123 (1.673)
I/σI	25.1 (2.5)	22.2 (2.2)	12.1 (1.5)
Completeness (%)	99.5 (97.7)	99.8 (99.8)	100.0 (100.0)
Redundancy	3.7 (3.7)	5.1 (5.1)	11.4 (11.4)
Refinement			
Resolution (Å)	40–2.9 (3.08-3.0)	30–2.4 (2.46-2.40)	30–2.8 (2.87-2.80)
No. reflections	7751	25786	17329
σ cutoff	none	none	none
R_{work}/R_{free}	0.186/0.260 (0.288/0.437)	0.171/0.202 (0.257/0/331)	0.180/0.21.9 (0.356/0.444)
No. atoms			
Protein	3123	3186	3265
Ligand/ion	4	4	4
Solvent	14	152	7
Average B-factors			
Protein	101.8	60.3	85.6
Ligand/ion	107.6	57.9	87.5
Water	67.9	65.0	68.9
R.m.s. deviations			
Bond lengths (Å)	0.005	0.005	0.007
Bond angles (°)	0.91	1.03	1.16